Efficient Photochemical Merocyanine-to-Spiropyran Ring Closure Mechanism through an Extended Conical Intersection Seam. A Model CASSCF/CASPT2 Study

Isabel Gómez, Mar Reguero,* and Michael A. Robb

Department Química Física i Inorgánica, Universitat Rovira i Virgili, C. Marcel·lí Domingo s/n, Tarragona 43007, Spain, and Chemistry Department, Imperial College London, London SW7 2AZ, U.K.

Received: October 28, 2005; In Final Form: January 27, 2006

A mechanism of the thermal and photochemical bleaching of merocyanine to spiropyran is proposed on the basis of CASSCF/CASPT2 calculations on the 6-(2-propenyliden)cyclohexadienone model system. Our results suggest that this photochemical transformation takes place in two steps. First, the initially pumped $^1(\pi-\pi^*)$ S_2 undergoes radiationless decay to $^1(n-\pi^*)$ S_1 via an extended S_2/S_1 conical intersection seam that runs approximately parallel to the trans-to-cis isomerization coordinate, a few kilocalories per mole higher in energy. Thus, $S_2 \rightarrow S_1$ internal conversion is possible at all values of the S_2 trans-to-cis reaction coordinate. Second, on the S_1 potential energy surface, there is a barrierless ring closure reaction path from the S_1 cis minimum that leads to a peaked S_1/S_0 conical intersection where the deactivation to the ground state takes place. The inertia of the moving nuclei then drives the system toward the ground-state minimum of the 2H-chromene product. Thus, the extended seam topology of the S_2/S_1 conical intersection and the coordinate of the branching space of the S_1/S_0 conical intersection are essential to explain the efficiency and high speed of this reaction.

Introduction

Since their discovery by Fischer and Hirshberg,[1] photochromic molecules have received much attention recently because of their wide-ranging industrial applications such as in ophthalmic glasses, optical switches, optical memories, and nonlinear optical devices.[2−17]

In this paper, we computationally study the photochemical bleaching reaction of a simple system—the 2H-chromene—as a model for larger spiropyrans. We show how the topology of the conical intersections involved in the reaction mechanism is crucial to explaining the high efficiency and speed of the reaction studied.

Despite the many classes of organic photochromic materials, the chemistry of the spiro-type compounds is one of the most extensively documented, because these compounds undergo light-activated photoisomerization reactions that can be applied to photoswitching processes.[18−20] Spiro-type compounds mainly consist of two planar heterocycles joined by a common tetrahedral carbon atom that imposes the orthogonality between these heterocycles and prevents the conjugation of the two π-electronic systems. Consequently, the spiropyran (SP) compounds are practically colorless, since the lowest electronic transition takes place in the region of the near-ultraviolet ($\lambda <$ 400 nm). This excitation produces the break of the C−O spiro bond in an excited singlet state in a few picoseconds.[21−25] The subsequent rotation across the C−C bond leads to an open photoisomer, called merocyanine (MC), which absorbs strongly in the visible region ($\lambda = 500-700$ nm) because of the π-electronic delocalitation by conjugation. Opposite to the closed forms, these photoisomers show an intense coloration and a high dipole moment. When the irradiation stops, the system can return to its original state, either thermally or via visible irradiation

SCHEME 1

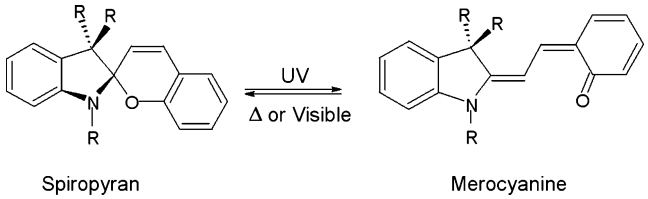

Spiropyran Merocyanine

(Scheme 1). This latter process is also an ultrafast reaction, occurring in less than 200 fs.[26] Some experimental and theoretical studies have analyzed the mechanism involved in the photochromism of these molecules,[27−33] but they have either focused just on the photochemical ring-opening process or on the thermal bleaching, while the photochemical ring-closure mechanism and the intermediates involved in this reaction are still a mystery.

Merocyanine has eight different stereoisomers from the various possible conformations of the central C−C bonds. The isomers detected experimentally in solution correspond mainly to the TTC and TTT configurations,[34−36] where T and C indicate trans and cis conformations of the C−C bonds in the methine bridge. The results obtained by Bahr[37] in his experiments of time-resolved fluorescence suggest that there are at least four different excited isomers in the MC structure with lifetimes of 15 ps, 45 ps, 120 ps, and 2 ns. What, therefore, is the role of photoisomerization in the process from photoexcited MC to SP? Since the cis conformation of the merocyanine is the precursor of the closed form of the spiropyran, and given the rate of the process, the conversion of the isomeric trans-MC to the cis-MC must happen via a low-energy route with the sequential rotation of the three central dihedral angles.

The two constituent π-electron systems do not interact significantly in the SP structure, so the absorption spectrum of the spiropyran compounds is approximately the superposition

* mar.reguero@urv.net.

10.1021/jp056208u CCC: $33.50 © 2006 American Chemical Society
Published on Web 02/28/2006

SCHEME 2

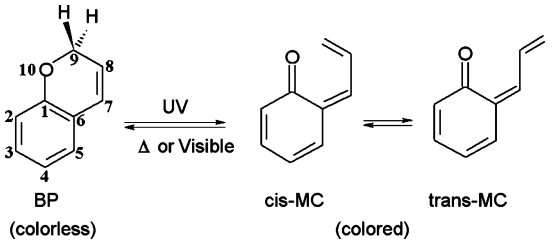

of the spectra of the two individual moieties.[38,39] In 1966, Becker et al. showed that the chromene-only half of the spiropyrans is photochromic: photoexcitation at low temperatures of the colorless 2H-chromene (or 2H-benzopyran, represented by BP) caused C−O bond cleavage, which resulted in a distribution of the isomers of the open colored structure—the 6-(2-propenyliden)cyclohexadienone (represented by MC as a model of the merocyanine), which reverted back to the original closed structure either thermally or photochemically (Scheme 2).[40] These results support the use of benzopyrans as a model for studying the photochromism of spiropyrans. Using benzopyrans reduces and simplifies the problem, because the eight possible conformations of the open form are reduced to the only two possibilities provided by the cis and trans isomers. After Becker's paper, many experimental[41−50] and theoretical[51−53] works studied the photochromic behavior of 2H-chromene derivatives under UV irradiation. One of the authors of the present work (M. A. Robb) studied the photochemical C−O bond cleavage reaction of the 2H-chromene to give the 6-(2-propenyliden)cyclohexadienone using CASSCF calculations and showed that the reaction takes place along the (n−π*) excited state, where the system ends up after the initial excitation, and decays to the ground state of the product through a conical intersection.

Neither this study nor the other theoretical studies investigated the opposite reaction—the ring-closure of the MC, and there is very little experimental information in the literature. Two points make such a study more difficult. First, the state pumped with the initial excitation is the S_2 ($\pi-\pi$*) state (as we will see later), so the decay to the S_1 (n−π*) reactive state must be documented. Second, the trans-to-cis isomerization of the open form must occur before the closure of the ring, and must also be studied.

In this paper, we report ab initio calculations at the CASSCF/CASPT2 level on the thermal and photochemical MC → BP conversion (including the trans-MC → cis-MC photoisomerization) on the merocyanine in order to shed light on the photochemical ring-closure mechanism and the species involved in it. We first study the thermal ground-state reaction and then analyze the trans-to-cis reaction on the open isomer of the 2H-chromene and the deactivation mechanism from the S_2 to the S_1 excited state. Finally, we study the ring-closure reaction, in which the system changes from the S_1 PES of the reactant to the S_0 PES of the product. As we mentioned earlier, we will show that two conical intersections with very different topologies are involved in the reaction. While the first one arises from the crossing of the S_2/S_1 potential energy surfaces and its seam runs parallel to the trans-to-cis isomerization path, the second one involves the S_1/S_0 states and is shaped like a funnel. The system reaches this funnel from a nearby transition state. The gradient from this critical point involves a reaction coordinate that takes the system to the product valley when decaying across the conical intersection. In short, the characteristics of the CIs are key to explaining the high efficiency of the reaction studied.

Computational Details

The ground state and the lower singlet excited states of the open form of 2H-benzopyrane have been studied with the complete active space self-consistent field (CASSCF)[54] method using a 6-31G(d) basis set.[55] The 12 electrons and 11 orbitals that constitute the active space include the π and π* orbitals of the ethylene and carbonyl fragments, together with the nonbonding pair of the oxygen atom of the carbonyl group. Full geometry optimizations were performed without any symmetry constraint. Numerical frequency calculations were calculated to determine the nature of the stationary points. Intrinsic reaction coordinates (IRCs)[56] were also computed to determine the pathways linking the critical structures (stationary points and conical intersections).

To incorporate the effect of the dynamical valence-electron correlation on the relative energies of the lower excited states, we performed second-order multiconfigurational perturbation theory calculations based on the CASSCF(12,11) reference function (CASPT2).[57] CASPT2 single-point energies were calculated at the CASSCF(12,11)/6-31G(d) optimized geometries, both with the same basis set (6-31G(d)) and with the more flexible basis set, the Dunning correlation consistent polarized valence double-ζ [9s4p1d/3s2p1d] basis set for carbon and oxygen, and [4s1p/2s1p] for hydrogen, designated cc-pVDZ.[58] All valence electrons were correlated. In the Results and Discussion section, the quantitative results used for the discussion will be the CASSCF(12,11)/6-31G(d)/CASPT2(12,-11)/cc-pVDZ ones unless the opposite is explicitly stated.

The CASPT2 calculations were performed using an average of states between the three singlet states of lower energy $S_0/S_1/S_2$. However, as in some zones of the potential energy surfaces the S_1 and S_2 states are almost degenerated and very high with respect to the ground state, we also used an average of 0.5/0.5 between the S_1/S_2 states. For the S_0/S_1 conical intersection, we used an average of 0.5/0.5. All CASPT2 computations were performed using the completed Fock matrix in the definition of the zero-order Hamiltonian, together with an imaginary level shift of 0.2 in order to prevent the incorporation of intruder states.[59]

CAS state interaction method (CASSI)[60] was used to compute the transition dipole moments of the various excited states in the Franck−Condon region. These, and the excitation energies, were used to obtain the values of the oscillator strength.

Conical intersections were optimized using the algorithm described in ref 61. State-averaged orbitals were used, and the orbital rotation derivative correction (which is usually small) to the gradient was not computed. This gives the lowest-energy point on the crossing, where there are two coordinates, the gradient difference and derivative coupling vectors (branching space), which lift the degeneracy. The remaining $3N - 8$ coordinates (intersection space) preserve the degeneracy, which therefore persists over a wide range of molecular geometries. Decay can take place away from the minimum-energy point on the crossing, depending on the kinetic energy of the system.

VB structures were determined by exploiting the results of the computation of the second-order exchange density matrix P_{ij} and the diagonal elements of the electronic density matrix (see ref 62 for details). The elements of P_{ij} have a simple physical interpretation, which is related to the spin coupling between the electrons localized in the orbitals residing on atoms i and j.[63] An illustration of the meaning of these matrix elements can be found in ref 62.

TABLE 1: Absorption Energies (ΔE, kcal mol^{-1}) and Oscillator Strengths (f) for the Two MC Isomers

	trans-MC				cis-MC			
state	ΔE^a CASSCF	ΔE^a CASPT2	ΔE^b CASPT2	f^c	ΔE^a CASSCF	ΔE^a CASPT2	ΔE^b CASPT2	f^c
S_0	0.0	0.0	0.0		1.5	6.2	5.6	
S_1	84.4	62.3	60.7	0.044	75.2	66.1	63.7	0.010
S_2	95.5	76.0	74.2	0.332	98.5	85.1	83.0	0.214

[a] Results obtained using an $S_0/S_1/S_2$ state average and 6-31G(d) basis set. [b] Results obtained using an $S_0/S_1/S_2$ state average and cc-pVDZ basis set. [c] Values of the oscillator strength obtained with the CASSCF transition dipole moments and excitation energies.

The CASSCF calculations were carried out with the *Gaussian 03* system of programs,[64] while the CASSI and CASPT2 computations were performed with the MOLCAS 6.0 program package.[65]

Results and Discussion

A. Thermal Reaction. To study the thermal reaction, we obtained the ground-state potential energy surface along the reaction path that connects reactants and products. When the energetics of the stationary points located at the CASSCF level were recalculated at the CASPT2 level, the trans-MC isomer was found to be 5.6 (6.9 at the CASSCF) kcal mol^{-1} more stable than the cis-MC isomer, which is in good agreement with the experimental data.[33−35] The computed barrier from the trans-MC to the cis-MC structure—8.6 (8.3 at the CASSCF level) kcal mol^{-1}—is small enough to permit a certain population of the cis-MC minimum. These three stationary structures show very similar geometries with strongly localized C═C double bonds and a slightly polarized C_1═O double bond. Optimized geometries, VB structures, and values of the second-order exchange density matrix and the one electron density matrix are shown in Figures S1 and S2 of the Supporting Information.

A transition state connecting the cis-MC isomer with the BP product (labeled TS_{close}) with an O−C_9 distance of 2.058 Å was located. Its geometry and the transition vector are shown in Figure S3 of the Supporting Information. At the CASPT2 level, this structure is 6.6 kcal mol^{-1} above the cis-MC minimum. The colorless BP product (whose geometry is shown in Figure S4 of the Supporting Information) is 27.6 kcal mol^{-1} more stable than the cis-MC isomer. Thus, the barrier of the associated inverse process, BP → cis-MC, is 34.2 kcal/mol high. This is in good agreement with the experimental observation that the MC structures evolve to the SP in 20−800 s even at low temperatures, while the opposite reaction is only possible after an initial photoexcitation.[36]

B. Initial Excitation and MC S_2 to S_1 Decay. First, vertical excitations from the ground-state trans- and cis-MC minima to the S_1 and S_2 excited states were calculated together with the corresponding oscillator strengths. Table 1 shows the results. The first excited state has an (n−π^*) character, while the second excited state has a ($\pi-\pi^*$) character. The values of the oscillator strength (columns 5 and 9 of Table 1) indicate that the excitation is mainly due to absorption to the S_2 state that corresponds to an energy of around 95−99 kcal mol^{-1}. The experimental values of the absorption energies of different merocyanine derivatives are in the 500−700 nm range (41−58 kcal/mol),[18−37] which are significantly lower than the values of $\Delta E_{S_0-S_2}$ obtained in this study. However, one must take into account that we are comparing the values of a large system with the results of a model system.

For both excited states, trans-MC and cis-MC minima were located together with their connecting transition state. The trans-to-cis isomerization path found on the ground-state potential energy surface was reproduced on the first two excited states in such a way that the three surfaces, S_0, S_1, and S_2, were more or less parallel. The energies obtained at several levels of theory for the stationary points located are shown in Table 2. Their geometries, VB electronic structures, second-order density matrices, and one-electron density matrices are illustrated in Figures S5 and S6 of the Supporting Information.

TABLE 2: Relative Energies (ΔE, kcal/mol) and Dipole Moments (μ, D) of the Different Structures Involved in the MC → BP Process, Calculated at Different Levels of Theory[a]

structure	ΔE^b CASSCF 6-31G(d)	ΔE^c CASPT2 6-31G(d)	ΔE^c CASPT2 cc-pVDZ	μ^b
S_0-trans	0.0	0.0	0.0	2.6
S_1(n−π^*)-trans	50.2	42.2	43.8	1.5
S_2($\pi-\pi^*$)-trans	72.7	54.5	52.6	3.9
S_0-cis	6.9	6.2	5.6	2.6
S_1(n−π^*)-cis	54.3	45.2	45.1	1.4
S_2($\pi-\pi^*$)-cis	77.7	59.4	57.6	3.8
S_0-$TS_{cis/trans}$	8.3	8.4	8.6	2.7
S_1(n−π^*)-$TS_{cis/trans}$	60.1	52.5	54.9	1.5
S_2($\pi-\pi^*$)-$TS_{cis/trans}$	91.1	75.2	73.8	3.8
CI−$S_1/S_{2\,(trans)}$	86.4	[60.2, 60.6]	[58.8, 59.7]	1.9
CI−$S_1/S_{2\,(TS)}$	107.0	[77.5, 78.4]	[77.3,78.8]	2.1
CI−$S_1/S_{2\,(cis)}$	98.6	[67.1, 72.6]	[66.5, 72.3]	1.5
S_0-TS_{close}	31.8	12.0	12.2	1.2
S_1(n−π^*)-TS_{close}	56.6	44.8	44.7	1.2
CI−S_0/S_1	52.0	[28.7, 36.4]	[28.2, 36.9]	2.0
S_0-BP	−10.3	−23.7	−22.0	1.4
S_1($\pi-\pi^*$)-BP	92.0	67.2	66.0	1.0

[a] The numbers in brackets correspond to the breaking of the degeneracy when the energies are calculated at the CASPT2 level at the CASSCF optimized CI geometries. [b] Two-state average used at the conical intersections. [c] Three-state average used except at the conical intersections where two-state average was used.

To obtain the initial relaxation path on the excited-state surfaces, a profile of the S_1 and S_2 surfaces was calculated at the CASPT2/6-31G(d) level by linear interpolation between the Frank−Condon region and the S_2 trans minimum. The results are shown in Figure 1. We can see that the relaxation to the S_2 trans minimum is a direct process. The most important feature, though, is the degeneracy that appears between the first and second excited states. This is located near the S_2 trans minimum (geometry optimized at the CASSCF level). The energy gap from the minimum to this point of degeneracy cannot be calculated accurately because of the impossibility of optimizing geometries at the CASPT2 level. Nevertheless, in view of the results shown in Figure 1, our guess is that the degeneracy must be at most only a few kilocalories per mole above the S_2 trans minimum.

When searching for the minimum of the S_1/S_2 conical intersection at the CASSCF level, we found three local minima in the vicinity of the $TS_{cis/trans}$ and the cis- and trans-MC minima. The energies of these minima are listed in Table 2, and the geometries are shown in Figure S7 of the Supporting Information. For the three minima, the coordinates of the branching space, the gradient difference, and the derivative coupling vectors were almost parallel, so the CI hypersurface is in this

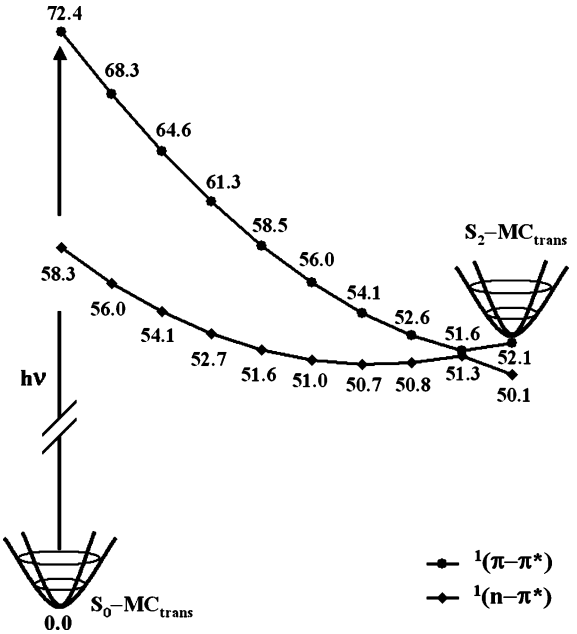

Figure 1. Energy profiles for S_1 and S_2 potential energy surfaces from the S_0 trans minimum geometry to the S_2 trans minimum. These were obtained by a linear synchronous transit path at the CASSCF(12,11)/CASPT2/6-31G(d) level using state-average of 0.5/0.5 for S_1/S_2 states. All the energies are in kcal mol^{-1}.

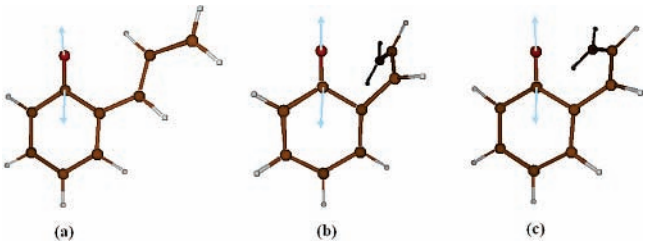

Figure 2. Branching space vector at the minima of the S_1/S_2 conical intersection located on the (a) trans-MC region, (b) $TS_{cis/trans}$ region and (c) cis-MC region.

case N-1-dimensional. The only coordinate of the branching space (of the CI minima located in the area of the trans-MC, $TS_{cis/trans}$, and cis-MC) is shown in Figure 2. The main component of this coordinate corresponds to the enlargement of the C_{1-O} distance. This is shorter at the CI geometries than at the S_1 and S_2 minima, which implies that the minima of both surfaces are in the same direction from the CI, i.e., it is a sloped CI. The monodimensional branching space includes only skeletal deformations, which ensures that the CI seam extends along the trans-MC → cis-MC path. A 3D representation of this seam can be found in Figure 3. Energetically, the CI is not very high above the isomerization path—no more than 15 kcal mol^{-1} when the CASPT2 energies are calculated at the CASSCF optimized geometries. However, as we have already commented when discussing the results shown in Figure 1, there are more accessible points from the isomerization path to the intersection hyperline than those given by the CASSCF optimized geometries (e.g., the CI must be only a very few kcal mol^{-1} above the S_2 trans minimum). The existence of this seam all along the trans/cis-MC isomerization path ensures an efficient and fast decay from the pumped state at the initial excitation (the ($\pi-\pi^*$) S_2 state) to the reactive state (the ($n-\pi^*$) S_1 state).

C. S_1 MC-to-BP Reaction Path. The closure of the second ring that yields the BP closed structure implies the formation of an O−C_9 σ bond. The orbital of the oxygen oriented in the appropriate direction to form such a bond is the n orbital, so in

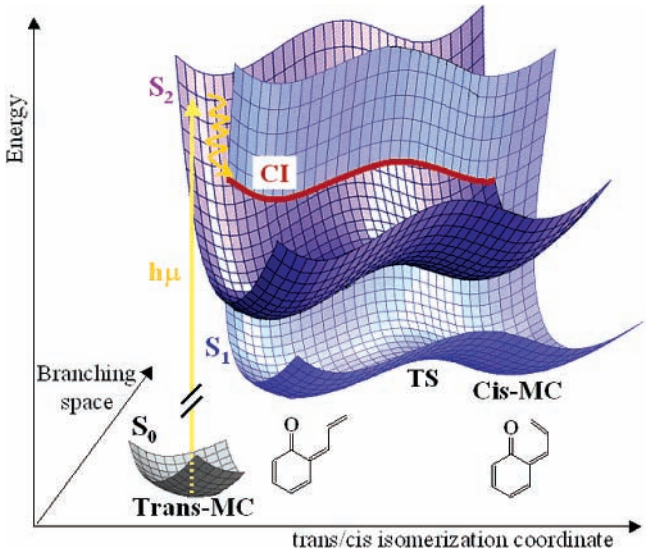

Figure 3. 3D representation of the photoisomerization pathway and the extended seam of the conical intersection between the S_1 and S_2 potential energy surfaces on the MC region.

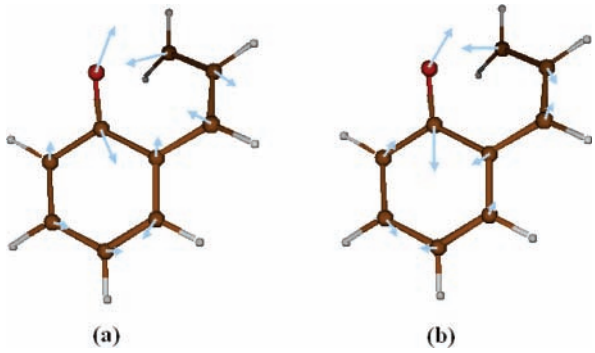

Figure 4. Branching space coordinates of the S_1/S_0 conical intersection: (a) the derivative coupling vector and (b) the gradient difference vector.

the product ground state, the electron density over it must add up to 1. This means that the electron distribution of the ground-state products corresponds to the $^1(n-\pi^*)$ excited state of the reactant, so a S_1/S_0 crossing must occur in the MC-to-BP reaction path. According to this hypothesis, a minimum on the S_1/S_0 CI was located at a geometry with a O−C_1 distance of 1.317 Å, which is intermediate between the values at the S_1-cis MC minimum and at the S_0-BP product. This geometry is shown in Figure S8 of the Supporting Information. This intersection is lower in energy than the S_1-cis minimum, and the branching space, shown in Figure 4, is mainly defined by O−C_1 bond elongation and C_7-C_8 bond shortening. This CI is the same as the one found in the previous study of the backward reaction of the opening of the BP cycle.[51] As we can see in the 3D representation shown in Figure 5, it has a peaked character.

The S_1 cis-MC isomer is obviously a precursor of the BP closed form, so the reaction path over the $^1(n-\pi^*)$ excited state should be documented.

The results in Table 2 show that the trans-to-cis isomerization path implies a barrier of 11.1 kcal mol^{-1}, which is easily surmountable with the kinetic energy accumulated after the initial excitation to the S_2 surface and subsequent decay. Between the cis-MC minimum and the S_1/S_0 CI, a TS was located at the CASSCF level on the S_1 surface. Its geometry is shown in Figure S9 of the Supporting Information. At this level of theory, this TS implies a barrier of 2.3 kcal mol^{-1} from the S_1-cis minimum. As we can see in Figure 6, the main component

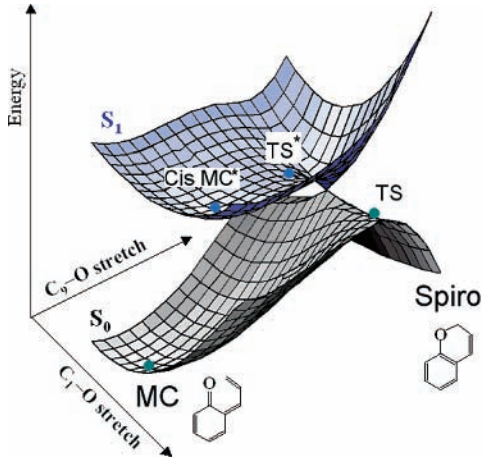

Figure 5. 3D representation of the conical intersection between the S_0 and S_1 potential energy surfaces in the space of the two main internal coordinates involved in the MC → BP reaction.

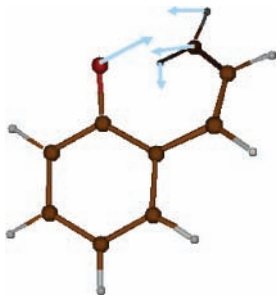

Figure 6. Transition vector of the S_1 transition state that connects cis-MC and BP.

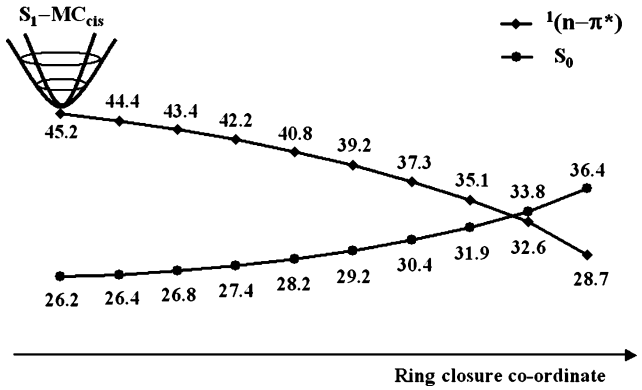

Figure 7. Energy profile for the S_0 and S_1 potential energy surfaces from the S_1-cis equilibrium geometry to the CI−S_0/S_1 conical intersection minimum geometry optimized at the CASSCF level. The profiles were obtained by a linear synchronous transit path at the CASSCF-(12,11)/CASPT2/6-31G(d) level using state-average 0.5/0.5 for S_0/S_1 states. All energies are in kcal mol^{-1}.

of the transition vector is the rotation around the C_8-C_9 bond, which orientates the p orbital of C_9 in a suitable direction to form the σ bond with the oxygen atom. A small component of $O-C_1$ bond elongation is also found.

When the energy of this TS was recalculated at the CASPT2 level, this critical point was located 0.4 kcal mol^{-1} below the S_1-cis minimum. To clarify the topology of the CASPT2 surface in this region, we calculated the profile of the S_0 and S_1 potential energy surfaces between the S_1-cis minimum and the S_1/S_0−CI at the CASPT2/6-31G(d) level. These results are shown in Figure 7, where the S_1/S_0 crossing has clearly been shifted to a different geometry and energy. At the CASPT2/6-31G(d) level, the crossing is 12.6 kcal mol^{-1} lower than the S_1-cis minimum. The path from this minimum to the CI seems to be a barrierless process, but we should bear in mind that the location of the minimum at the CASPT2 level may also be different, and a barrier does in fact exist. In any case, it must be quite small—smaller in fact than the previous trans-to-cis barrier and the initial excitation.

The passage along the TS located at CASSCF (following the transition vector) or downhill from the minimum implies an elongation of the $O-C_1$ bond distance and a shortening of the $O-C_9$ distance. When the system reaches the CI, the nuclei will, because of inertia, continue the same movement. As these are the main components of the branching space vector, the system will leave the degeneracy very rapidly toward the valley of the product. The reaction will yield the BP closed form quickly and efficiently.

Finally, the S_1−BP minimum was also located, 88.0 kcal mol^{-1} above the ground-state BP. This structure will not be further discussed, as it is crucial only in the photochemical BP-to-MC process, and a detailed study on this reaction has already been published.[51]

Conclusions

In accordance with these calculations, we propose the following mechanistic interpretation:

Irrespective of the conformation of the reactant, the absorption of the initial excitation promotes the system to the S_2 excited state that has a ($\pi-\pi^*$) character. An equilibrium between the trans- and cis-MC isomers could be established on this potential energy surface, but a very efficient nonadiabatic path to the S_1 state, that has an (n−π^*) character, is open all the way along the isomerization path. The seam of a S_2/S_1 conical intersection runs parallel to this path at accessible energies, so the radiationless decay can take place at any rotational angle around the C_7-C_8 bond, and the internal conversion will be very fast. Once on the S_1 surface, again the trans−cis equilibrium may be established, but from the cis minimum, a low-barrier path leads to a S_1/S_0 conical intersection. The initial movement of the nuclei will lead the system through the CI to the ground state of the BP product in a very fast second step of the reaction.

Acknowledgment. This work has been supported by grant number BQU2002-04029-C02-02 of the Spanish Ministerio de Ciencia y Tecnología.

Supporting Information Available: Geometrical parameters of all the critical points located. Values of the second-order exchange density matrix and the one-electron density matrix of the trans- and cis-MC minima and the connecting TS located on the S_0, S_1, and S_2 potential energy surfaces. This material is available free of charge via the Internet at http://pubs.acs.org.

References and Notes

(1) Fischer, E.; Hirshberg, Y. *J. Chem. Soc.* **1952**, 4522.

(2) Kelly, J. M., McArdle, C. B., Maunder, M. J. de F., Eds. *Photochemistry and Polymeric Systems*; The Royal Society of Chemistry, Cambridge, 1993.

(3) Perrott, C.; Pidgeon, K. J. PCT, WO 96 18 927; *Chem. Abstr*. **1996**, *125*, 93652.

(4) Crano, J. C.; Flood, T.; Knowles, D.; Kumar, A.; Gemert, B. V. *Pure Appl. Chem*. **1996**, *68*, 1395.

(5) Tschochner, R. Ger. Offen DE 19,643,773; *Chem. Abstr*. **1964**, *128*, 283583.

(6) Hou, L. S.; Schmidt, H. *J. Mater. Sci. Lett.* **1997**, *16*, 435.

(7) Scaudel, B.; Guermeur, C.; Sanchez, C.; Nakatani, K.; Delaire, V. *J. Mater. Chem.* **1997**, *7*, 61.

(8) Yu, L. H.; Ming, Y. F.; Fan, M. G. *Sci. China, Ser. B* **1995**, *25*, 799.

(9) Wojtyk, J. T. C.; Kazmaier, P. M.; Buncel, E. *Chem. Commun*. **1998**, 1703.
(10) Winkler, J. D.; Bowen, C. M.; Michelet, V. *J. Am. Chem. Soc.* **1998**, *120*, 3237.
(11) Morrison, H., Ed. *Bioorganic Photochemistry*. *Biological Applications of Photochemical Switches*; Wiley: New York, 1993; Vol. 2.
(12) Willner, I.; Rubin, R.; *Angew. Chem., Int. Ed. Engl*. **1996**, *35*, 367.
(13) Hattori, S. Japanese Patent 98,110,162; *Chem. Abstr*. **1998**, *128*, 301912.
(14) Chan, Y. P. PCT, WO 97 10 241; *Chem. Abstr*. **1997**, *126*, 310306.
(15) Meng, J. B.; Li, X. L.; Wang, S. F.; Wang, Y. M.; Shi, Z. H.; Liu, J. Y.; Li, M. Z. Chinese Patent 1,182,114; *Chem. Abstr*. **1998**, *132*, 130063.
(16) Khairutdinov, R. F.; Giertz, K.; Hurst, J. K.; Voloshina, E. N.; Voloshin, N. A.; Minkin, V. I. *J. Am. Chem. Soc.* **1998**, *120*, 12707.
(17) Berkovic, G.; Krongauz, V.; Weiss, V. *Chem. Rev*. **2000**, *100*, 741.
(18) Bertelson, R. C. *Mol. Cryst. Liq. Cryst.* **1994**, *246*, 1.
(19) Desvergne, J. P.; Bouas-Laurent, H.; Deffieux, A. *Mol. Cryst. Liq. Cryst.* **1994**, *246*, 111.
(20) Schaffner, K.; Schmidt, R.; Brauer, H. D. *Mol. Cryst. Liq. Cryst.* **1994**, *246*, 119.
(21) Tamai, N.; Masuhara, H. *Chem. Phys. Lett.* **1992**, *191*, 189.
(22) Ernsting, N. P.; Engeland, T. A. *J. Phys. Chem.* **1991**, *95*, 5502.
(23) Aramaki, S.; Atkinson, G. H. *Chem. Phys. Lett.* **1990**, *170*, 181.
(24) Wilkinson, F.; Worrall, D. R.; Hobley, J.; Jansen, L.; Williams, S. L.; Langley, A. J.; Matousek, P. *J. Chem. Soc., Faraday Trans*. **1996**, *92*, 1331.
(25) Fan, M.; Ming, Y.; Liang, Y.; Zhang, X.; Jin, S.; Yao, S.; Lin, N. *J. Chem. Soc., Perkin Trans. 2* **1994**, 1387.
(26) Dürr, H., Bouas-Laurent, H., Eds. *Photochromism and Systems*; Elsevier: Amsterdam, 1990.
(27) Crano, J. C., Guglielmetti, J. R., Eds. *Organic Photochromic and Thermochromic Compounds*; Plenum Press: New York, 1999; Vols. 1 and 2.
(28) Balzani, V.; Venturi, M.; Credi, A. *Molecular Devices and Machines*; Wiley-VCH: Weinheim, 2003.
(29) Tamai, N.; Miyasaka, H. *Chem. Rev.* **2000**, *100*, 1875−1890.
(30) Minkin, V. I. *Chem. Rev.* **2004**, *104*, 2751−2776.
(31) Ward, M. D. *Chem. Ind.* **1997**, 640−645.
(32) Willner, I. *Acc. Chem. Res.* **1997**, *30*, 640−645.
(33) Hobley, J.; Malatesta, V.; Giroldini, W.; Stringo, W. *Phys. Chem. Chem. Phys.* **2000**, *2*, 53.
(34) Hobley, J.; Malatesta, V. *Phys. Chem. Chem. Phys.* **2000**, *2*, 57.
(35) Hobley, J.; Malatesta, V.; Millini, R.; Montanari, L.; Parker, W. O. *Phys. Chem. Chem. Phys.* **1999**, *1*, 3259.
(36) Bahr, J. L.; Kodis, G.; Garza, L.; Lin, S.; Moore, A. L. *J. Am. Chem. Soc.* **2001**, *123*, 7124−7133.
(37) Hobley, J.; Bletz, M.; Asahi, T.; Fukumura, H. *J. Phys. Chem. A* **2002**, *106*, 2265−2270.
(38) Tyer, N. W., Jr.; Becker, R. S. *J. Am. Chem. Soc.* **1970**, *92*, 1289.
(39) Tyer, N. W., Jr.; Becker, R. S. *J. Am. Chem. Soc.* **1970**, *92*, 1295.
(40) Becker, R. S.; Michl, J. *J. Am. Chem. Soc.* **1966**, *88*, 5931.
(41) Edwards, L.; Kolc, J.; Becker, R. S. *Photochem. Photobiol.* **1971**, *13*, 423.
(42) Padwa, A.; Au, A.; Lee, G. A.; Owens, W. *J. Org. Chem.* **1975**, *40*, 1142.
(43) Becker, R. S.; Dolan, E.; Balke, D. E. *J. Chem. Phys.* **1969**, *50*, 239.
(44) Lenoble, C.; Becker, R. S. *J. Photochem.* **1986**, *33*, 187.
(45) Van Gemert, B.; Bergomi, M.; Knowles, D. *Mol. Cryst. Liq. Cryst.* **1994**, *246*, 67.
(46) Pozzo, J.-L.; Samat, A.; Guglielmetti, R.; Lokshin, V.; Minkin, V. *Can. J. Chem.* **1996**, *74*, 1649.
(47) Aldoshin, S.; Chuev, I.; Utenyshev, A.; Filipenko, O.; Pozzo, J.-L.; Lokshin, V.; Guglielmetti, R. *Acta Crystallogr., Sect. C* **1996**, *52*, 1834.
(48) Luccioni-Houze, B.; Campredon, M.; Guglielmetti, R.; Giusti, G. *Mol. Cryst. Liq. Cryst.* **1997**, *297*, 161.
(49) Pozzo, J.-L.; Samat, A.; Guglielmetti, R.; Dubest, R.; Aubard, J. *Helv. Chim. Acta* **1997**, *80*, 725.
(50) Kolc, J.; Becker, R. S. *Photochem. Photobiol.* **1970**, *12*, 383.
(51) Celani, P.; Bernardi, F.; Olivucci, M.; Robb, M. A. *J. Am. Chem. Soc.* **1997**, *119*, 10815.
(52) Day, P. N.; Wang, Z.; Pachter, R. J. *Phys. Chem.* **1995**, *99*, 9730.
(53) Zerbetto, F.; Monti, S.; Orlandi, G. *J. Chem. Soc., Faraday Trans. 2* **1984**, *80*, 1513.
(54) For a review, see: Roos, B. O. *Adv. Chem. Phys.* **1987**, *69*, 399.
(55) (a) Herhe, W. J.; Ditchfield, R.; Pople, J. A. *J. Chem. Phys.* **1972**, *56*, 2257−2261. (b) Harihan, P. C.; Pople, J. A. *Theor. Chim. Acta* **1973**, *28*, 213−222.
(56) (a) Fukui, K. *Acc. Chem. Res.* **1981**, *14*, 363. (b) Schmidt, M. W.; Gordon, M. S.; Dupuis, M. *J. Am. Chem. Soc*. **1985**, *107*, 2585. (c) Gonzalez, C.; Schlegel, B. *J. Chem. Phys.* **1989**, *90*, 2154. (d) Gonzalez, C.; Schlegel, B. *J. Phys. Chem.* **1990**, *94*, 5523.
(57) (a) Anderson, K.; Malmqvist, P.-A.; Roos, B. O.; Sadlej, A. J.; Wolinski, K. *J. Phys. Chem*. **1990**, *94*, 5483. (b) Anderson, K.; Malmqvist, P.-A.; Roos, B. O. *J. Chem. Phys.* **1992**, *96*, 1218.
(58) Dunning, T. H. *J. Chem. Phys.* **1989**, *90*, 1007.
(59) (a) Roos, B. O.; Andersson, K. *Chem. Phys. Lett.* **1995**, *245*, 215. (b) Roos, B. O.; Andersson, K.; Fülscher, M. P.; Serrano-Andrés, L.; Pierloot, K.; Merchán, M.; Molina, V. *THEOCHEM* **1996**, *388*, 257.
(60) (a) Malmqvist, P.-Å. *Int. J. Quantum Chem.* **1986**, *30*, 479. (b) Malmqvist, P.-Å.; Roos, B. O. *Chem. Phys. Lett.* **1989**, *155*, 189.
(61) (a) Celani, P.; Robb, M. A.; Garavelli, M.; Bernardi, F.; Olivucci, M. *Chem. Phys. Lett.* **1995**, *243*, 1−8. (b) Garavelli, M.; Celani, P.; Fato, M.; Bearpark, M. J.; Smith, B. R.; Olivucci, M.; Robb, M. A. *J. Phys. Chem. A* **1997**, *101*, 2023−2032.
(62) Blancafort, L.; Celani, P.; Bearpark, M. J.; Robb, M. A. *Theor. Chem. Acc.* **2003**, *110*, 92−99.
(63) McWeeny, R.; Sutcliffe, B. T. *Molecular Quantum Mechanics*; Academic Press: New York, 1969; pp 148−170.
(64) Frisch, M. J.; Trucks, G. W.; Schlegel, H. B.; Scuseria, G. E.; Robb, M. A.; Cheeseman, J. R.; Montgomery, J. A., Jr.; Vreven, T.; Kudin, K. N.; Burant, J. C.; Millam, J. M.; Iyengar, S. S.; Tomasi, J.; Barone, V.; Mennucci, B.; Cossi, M.; Scalmani, G.; Rega, N.; Petersson, G. A.; Nakatsuji, H.; Hada, M.; Ehara, M.; Toyota, K.; Fukuda, R.; Hasegawa, J.; Ishida, M.; Nakajima, T.; Honda, Y.; Kitao, O.; Nakai, H.; Klene, M.; Li, X.; Knox, J. E.; Hratchian, H. P.; Cross, J. B.; Bakken, V.; Adamo, C.; Jaramillo, J.; Gomperts, R.; Stratmann, R. E.; Yazyev, O.; Austin, A. J.; Cammi, R.; Pomelli, C.; Ochterski, J. W.; Ayala, P. Y.; Morokuma, K.; Voth, G. A.; Salvador, P.; Dannenberg, J. J.; Zakrzewski, V. G.; Dapprich, S.; Daniels, A. D.; Strain, M. C.; Farkas, O.; Malick, D. K.; Rabuck, A. D.; Raghavachari, K.; Foresman, J. B.; Ortiz, J. V.; Cui, Q.; Baboul, A. G.; Clifford, S.; Cioslowski, J.; Stefanov, B. B.; Liu, G.; Liashenko, A.; Piskorz, P.; Komaromi, I.; Martin, R. L.; Fox, D. J.; Keith, T.; Al-Laham, M. A.; Peng, C. Y.; Nanayakkara, A.; Challacombe, M.; Gill, P. M. W.; Johnson, B.; Chen, W.; Wong, M. W.; Gonzalez, C.; Pople, J. A. *Gaussian 03*, revision B.05; Gaussian, Inc.: Wallingford, CT, 2004.
(65) Andersson, K.; Barysz, M.; Bernhardsson, A.; Blomberg, M. R. A.; Cooper, D. L.; Fleig, T.; Fülscher, M. P.; DeGraaf, C.; Hess, B. A.; Karlström, G.; Lindh, R.; Malmqvist, P.-Å.; Neográ dy, P.; Olsen, J.; Roos, B. O.; Sadlej, A. J.; Schütz, M.; Schimmelpfennig, B.; Seijo, L.; Serrano-Andrés, L.; Siegbahn, P. E. M.; Stålring, J.; Thorsteinsson, T.; Veryazov, V.; Widmark, P.-O. MOLCAS version 6.0, Department of Theoretical Chemistry, Lund University, Sweden (2004).